Electronic Supplementary Information for

Core-Shell Nano-hollow γ-Fe_2O_3@Graphene Hybrid Prepared through the Kirkendall Process as High Performance Anode Materials for Lithium Ion Battery

Jiangtao Hu‡, Jiaxin Zheng‡, Leilei Tian, Yandong Duan, Lingpiao Lin, Suihan Cui, Hao Peng, Tongchao Liu, Hua Guo, Xinwei Wang and Feng Pan*

School of Advanced Materials, Peking University, Peking University Shenzhen Graduate School, Shenzhen 518055, China

* Corresponding author: panfeng@pkusz.edu.cn

‡ J. Hu and J. Zheng contributed equally to this work.

Materials and methods

***Synthesis nano-hollow γ-Fe_2O_3@Graphene and α-Fe_2O_3*:** the commercial Prussion Blue (0.5 g) and glucose (0.15 g) were dispersed in distilled water and ethanol, and dispersed further by grinding in mortar. Then the mixture was heated to 80℃ for 8h in air dry oven. Hereafter, the obtained mixture was calcined at 650 °C in argon atmosphere. The carbon-coated iron nanoparticles were produced, during which the PB was decomposed from 237°C as shown in Fig. S3a while Fe nano-metals was produced by reduction of glucose decomposition, during which the layer FeC_x is generated at the 650 °C ,then to separate into layers of graphene and Fe nano-metals when cooling down to the room temperature , so that the graphene layer was generated to coat on the nano Fe particles shown in Fig. 1 (I-II）. After the furnace cooling naturally to room temperature and then exposing in air, the nano Fe particles was oxided by O_2 by a spontaneous combustion to transfer into nano-hollow γ-Fe_2O_3

shown in Fig. 1 (III). For comparisons, the above mixture of Prussion Blue and glucose was calcined at 650℃ in air for 6 hours to form α-Fe_2O_3.

The mechanism of the nano-hollow γ-Fe_2O_3 prepared from the nano-Fe nano-crystals at the room temperature should be belonged to a type of nanoscale Kirkendall based-process coupled with interfacial oxidation chemical reactions in air by the Cabrera and Mott effect.[1] Cabrera and Mott's lower-temperature oxidation effect occurs initially on the oxide surface on which oxygen atoms are adsorbed, and electrons can pass rapidly through the oxide by tunneling to establish an equilibrium between the nano-Fe metal's surfaces and adsorbed oxygen to create an electronic field in the thin oxide layer, which can pull metal ions through the oxide film (shown in Fig.1III). Then, small Kirkendall voids will generate when Fe atoms in the inside-shell nanoparticles migrate into the γ-Fe_2O_3 surface layer and then contribute to the formation of a new γ-Fe_2O_3 layer. The second stage is dominated by Fe atomic surface diffusion from the nano-Fe core material along the pore surface to the reaction front as the dominant material transport process because of a much lower activation energy of surface diffusion than bulk diffusion. After all Fe atoms are consumed to react with oxygen ion absorbed on the γ-Fe_2O_3 surface, nano-hollow γ-Fe_2O_3 can be formed as a result of the vacancy clustering in the core as shown in Fig. 1 (III).

Structure and Morphology Characterization: the crystallographic structures of the samples were characterized with X-ray diffraction (XRD, Bruker D8 Advance diffractometer using Cu Kα)). XPS analyses were performed using ESCALAB 250XL. The scanning electron microscopy (SEM) images were measured on ZEISS Supra 55. The micro-structure of γ-Fe_2O_3@graphene was studied by using transmission electron microscopy (FEI Tecnai G2

F20 S-Twin). Thermogravimetry analysis(TGA) data of γ-Fe_2O_3@ graphene was collected on a TGA/DSC1 system at a heating rate of 10°C/min under oxygen flow. Raman spectrum was recorded by iHR 320. The surface area was determined by nitrogen adsorption/desorption using the Brunauer–Emmett–Teller method (BET, Micromeritics ASAP 2020 HD88).

Electrochemical Performance Test : the working electrode was prepared by coating a slurry of active material (60 wt %), carbon black (30 wt %), and poly(vinylidene fluoride) binder (10 wt %) dissolved in N-methylpyrrolidine onto a copper foil, and then drying in vacuum at 110℃ for 12 h. The 2032 coin-type cells were finally assembled in an argon-filled glovebox , using pure lithium foil as the counter electrode and reference electrode, cell grand membrane as the separator, and 1 M $LiPF_6$ in a mixture of EC, DEC and DMC with a volume ratio of 1:1:1 as the electrolyte. Before the electrochemical measurement, the prepared cells were shelved for 6h. Galvanostatic discharge/charge tests were performed using a NEWARE battery cycler in the voltage range of 0.01-3.0 V (vs. Li^+/Li) at room temperature. The cyclic voltammetry (CV) results were recorded by a CHI 604E. The electrochemical impedance measurements were carried out on the batteries which were charged and discharged for different cycles. All the electrochemical measurements were performed at room temperature.

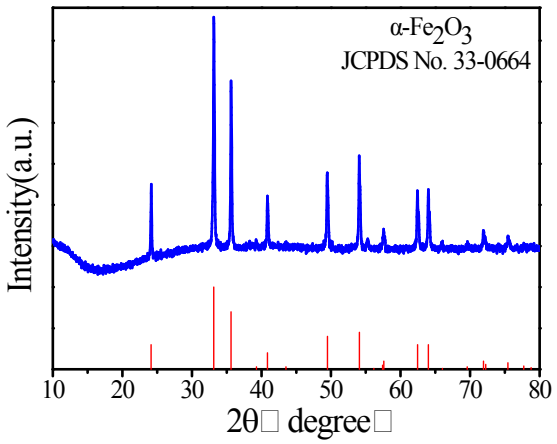

Figure S1. XRD pattern of the prepared α-Fe_2O_3.

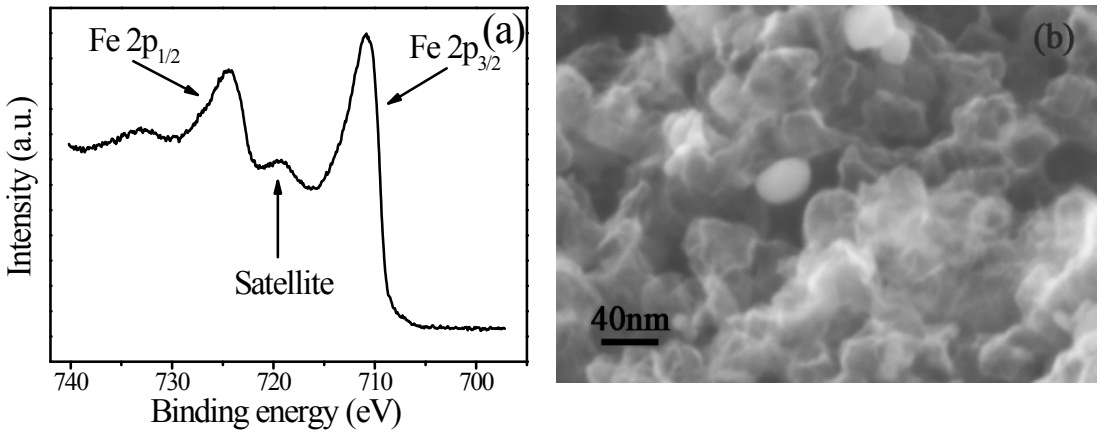

Figure S2. X-ray photoelectron spectroscopy (XPS) spectra: (a)Fe2p spectra, (b) the SEM image of the shell of the graphene left from nano-hollow γ-Fe2O3 @graphene dissolved in HCl.

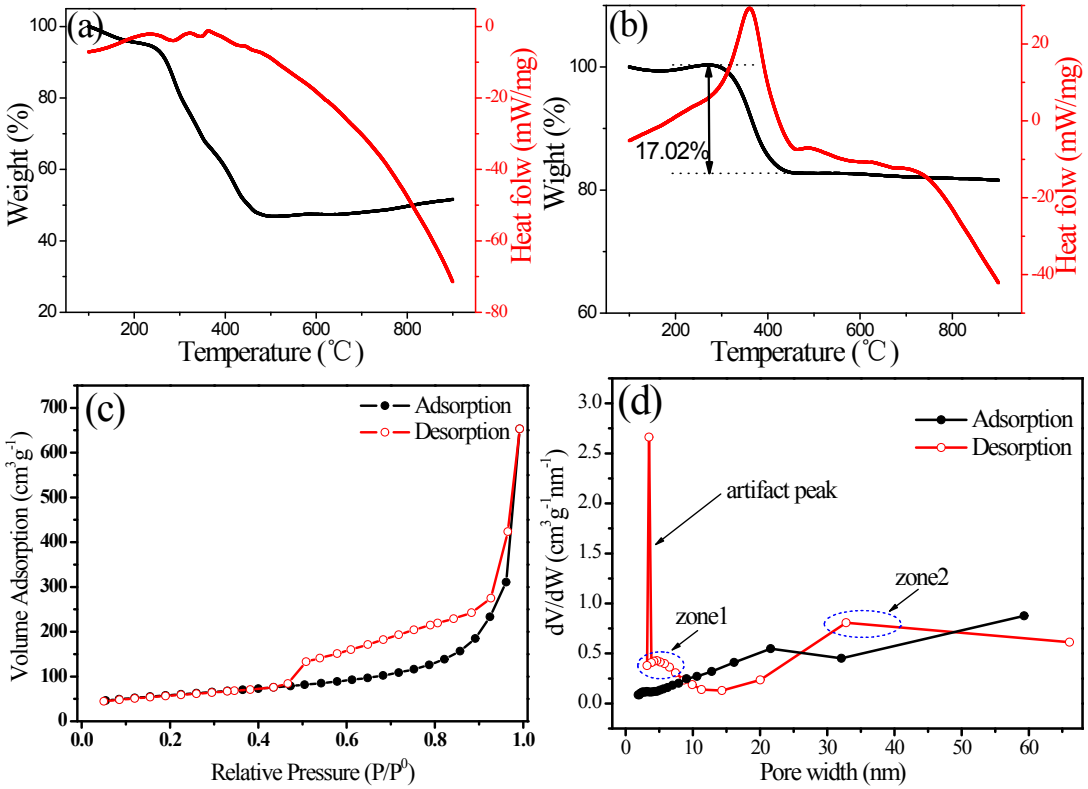

Figure S3. TGA and DTA curves of (a) PB in argon atmosphere and (b) nano-hollow γ-Fe_2O_3@graphene in oxygen atmosphere; (c) N_2-adsorption/desorption isotherms for nano-hollow γ-Fe_2O_3@graphene; (d) the pore size distribution (PSD) of γ-Fe_2O_3@ graphene depends on BJH method. The smaller pores, which are generated through the Kirkendall process, are distributed from 4-10 nm (peak around 5nm) marked as "zone 1" shown in the revised Fig. S3(d) as below. These pore sizes also match with TEM results shown in Fig. 1c.

The sharp peak in the PSD from the desorption branch is an artefact due to the intrinsic capillary evaporation of liquid nitrogen[2]. Another pore size (marked as "zone2 in Fig. S3d) is around 30nm ~ 40nm, which is generated by the packing pores of the core-shell γ-Fe2O3@graphene particles. From (c) and (d), it is clearly shown that the hybrid is a porosint with inhomogeneous nanoscale nanoporous and mesoporous.

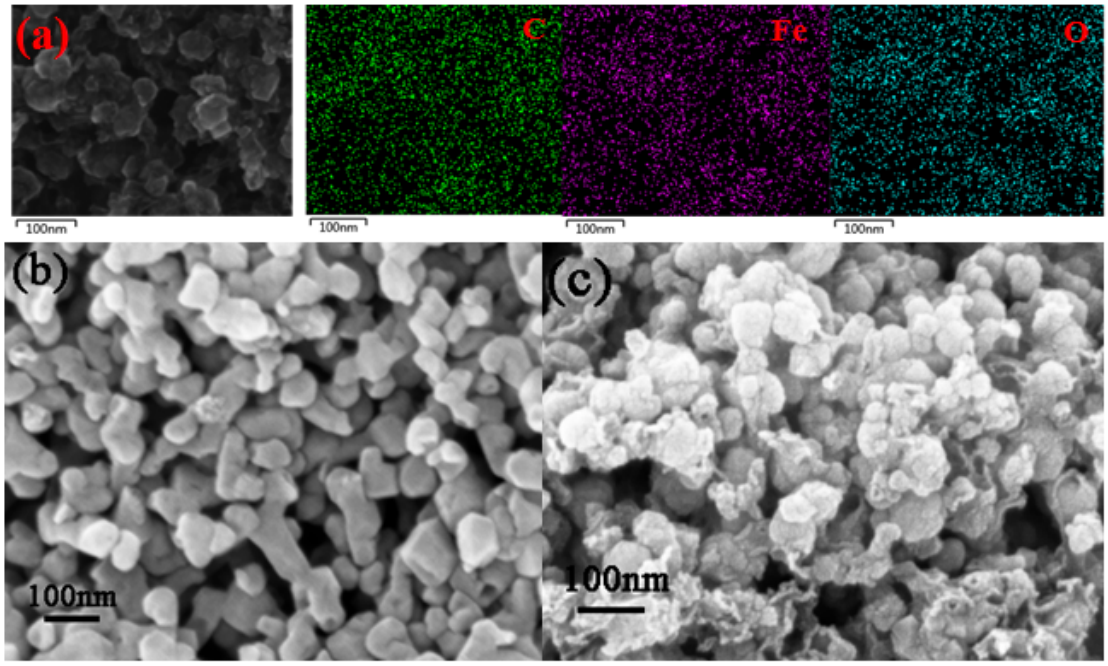

Figure S4. (a) The element mapping of nano-hollow γ-Fe_2O_3@graphene. SEM images of (b) Prussion Blue and (c) nano-hollow γ-Fe_2O_3@graphene.

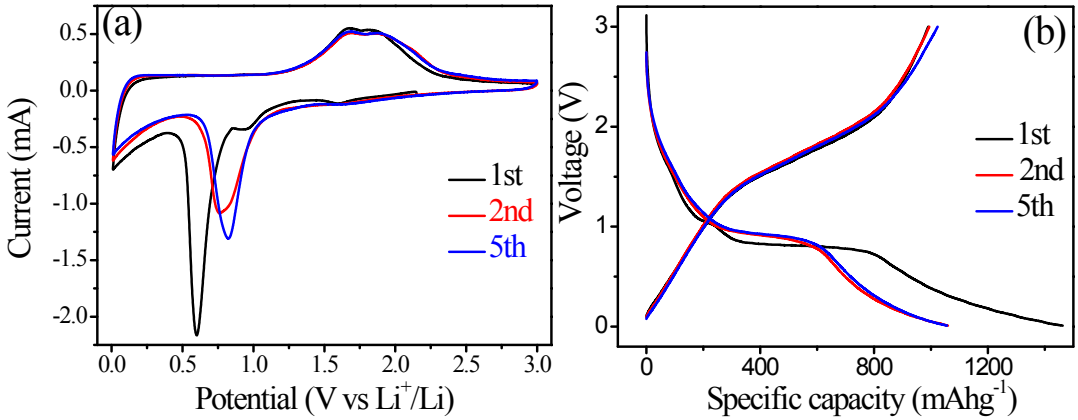

Figure S5. Electrochemical characterization of the prepared nano-hollow γ-Fe_2O_3@graphene: (a) cyclic voltammetry tests of nano-hollow γ-Fe_2O_3@graphene at 0.1C in the potential range of 0.01V to 3.0V (vs.Li/Li^+); (b) galvanostatic charge-discharge curves of nano-hollow γ-Fe_2O_3@graphene at 0.1C for the first 5 times.

Three obvious plateaus can be observed in the first discharge curve in Fig. S5b, which agree well with the three peaks in CV results for the first cycle. The following sloping region can be described as the formation of polymeric SEI layers. The first cycle discharge and charge capacities of nano-hollow γ-Fe_2O_3@graphene electrode at 0.1 C (1 C = 1000 mAg^{-1}) are 1462.32 and 990.45 mAh g^{-1}, respectively, corresponding to a coulombic efficiency of 67.73%, which can also be explained by the irreversible formation of the SEI layers on the surface of nano-hollow γ-Fe_2O_3@graphene particles.

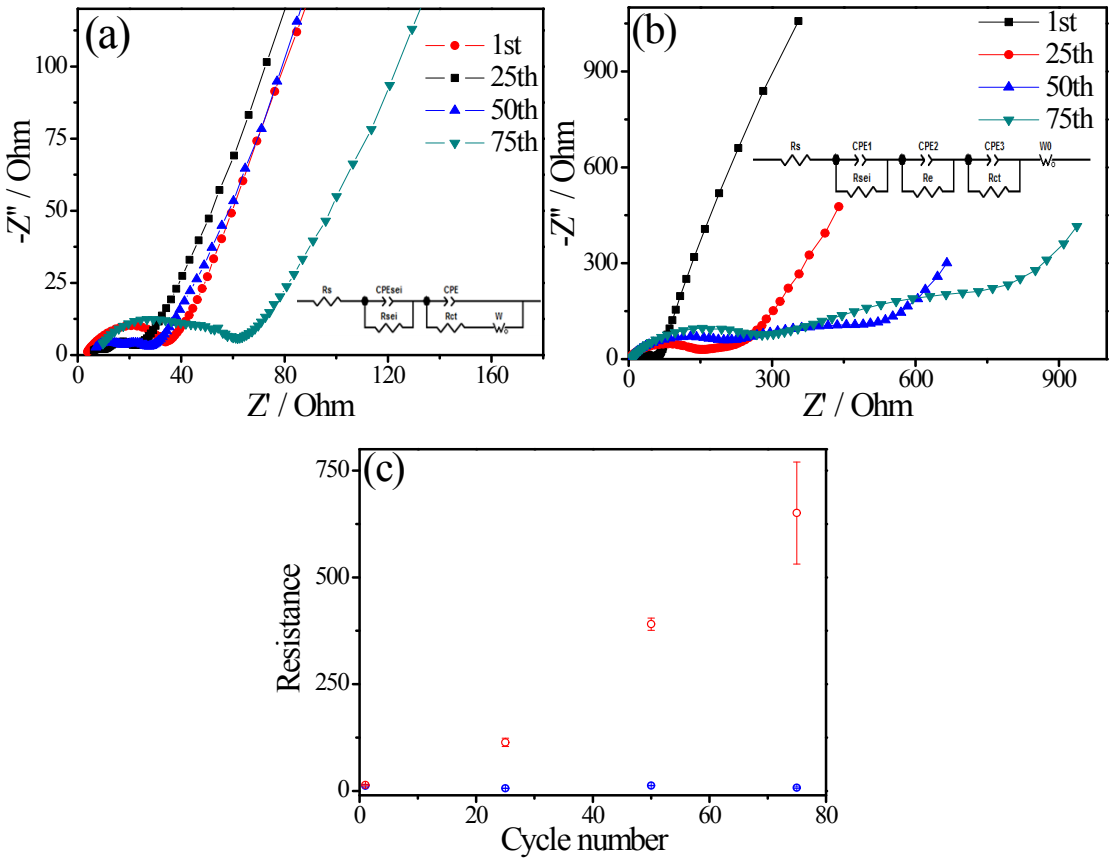

Figure S6. EIS data and equivalent circuit of (a) nano-hollow γ-Fe_2O_3@graphene and (b) *α*-Fe_2O_3; (c) charge transfer resistances and their errors calculated from impedance fitting of nano-hollow γ-Fe_2O_3@graphene (blue) and *α*-Fe_2O_3 (red).

Electrochemical impedance spectroscopy (EIS) measurements were performed after 1, 25, 50, and 75 charge/discharged cycles at 0.5 C for both nano-hollow γ-Fe_2O_3@graphene and α-Fe_2O_3 (Fig. S6). For nano-hollow γ-Fe_2O_3@graphene, the visible semicircles in the high and middle frequency ranges reflect the SEI (R_{SEI}) and charge transfer (R_{ct}) resistances, respectively. [3] But for α-Fe_2O_3, three semicircles are needed to describe the resistances sufficiently, representing the resistance of SEI, electron, and charge transfer, respectively. Fig. S6c shows the R_{ct} for the two materials from impedance fitting. The values of R_{ct} for both

materials become larger with the increasing number of cycles. It is also noticeable that the charge transfer resistances for nano-hollow γ-Fe_2O_3@graphene are much smaller and increase much slower with the increasing cycles number than those for α-Fe_2O_3, indicating a higher electrical conductivity induced by the graphene shells.

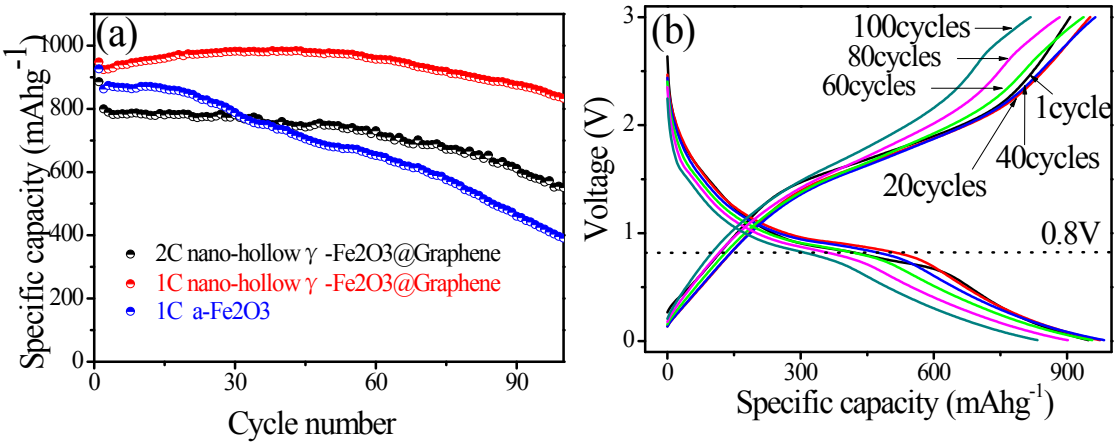

Figure S7. (a) Cycling performances of nano-hollow γ-Fe_2O_3@graphene at 1C and 2C and α-Fe_2O_3 at 1C; (b) the charge-discharge curves of nano-hollow γ-Fe_2O_3@graphene at 1C for 100 cycles.

The much better cycling stability of the nano-hollow γ-Fe_2O_3@graphene can be attributed to the structural stability of γ-Fe_2O_3 (the (400) peak still exists during the charge and discharge process) and the nano-hollow structure with graphene shells, which buffer the volume expansion during electrochemical cycles. While the structure of a-Fe_2O_3 was damaged by the volume expansion during charge and discharge cycles, due to the absence of hollow structures and the relatively low structure stability of a-Fe_2O_3 during electrochemical cycles.

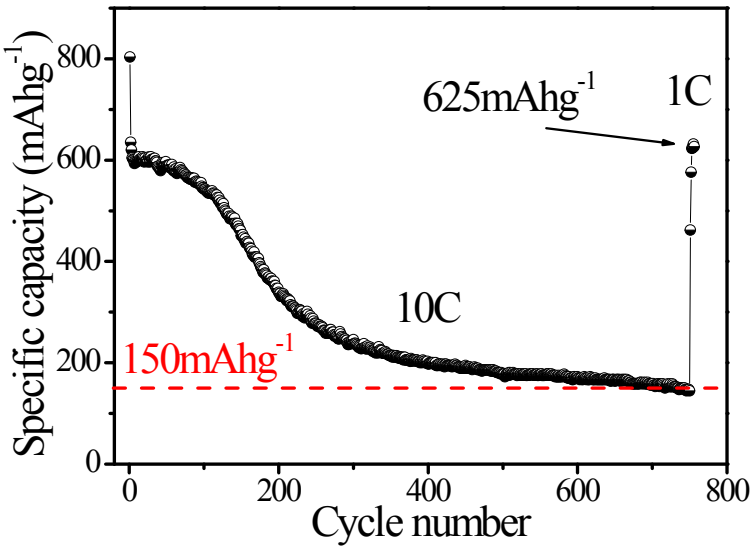

Figure S8. Galvanostatic charge-discharge curves of nano-hollow γ-Fe_2O_3@graphene at 10C for 750 cycles and 1C for 6 cycles. The dramatic drop after 100 cycles may be due to the significant increase of the electrical impedance.

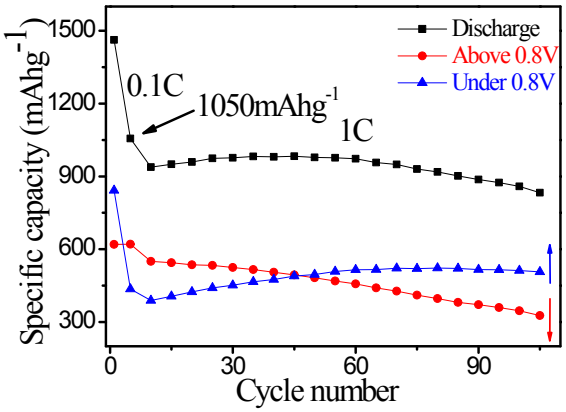

Figure S9. Schematic illustration of two parts of battery capacity of nano-hollow γ-Fe_2O_3@graphene at 0.1C and 1C between 0.01v and 3V, red curve stands for the capacity above 0.8V, blue curve stands for the capacity under 0.8V.

Table S1. The performance comparison of iron-based materials for lithium-ion batteries.

Ref.	Material	Morphology	Specific capacity	Rate-capacity
[4]	Fe_2O_3.carbon	a-Fe2O3 nanorods/CNFs	1C/446mAhg^{-1} and 2C/317 mAhg^{-1} for 30cycles	
[5]	Fe_2O_3-graphite	Nano-particle	0.1C/491mAhg^{-1} for 55cycles	1C/295 mAhg^{-1}
[6]	Fe_2O_3	Nano-composites	125mA g^{-1}/470 and 419mAhg-1 at80 and 200cycles	
[7]	α-Fe_2O_3@C	Core–shell nanotubes	1C/1012-4C/482mAhg-1 for 300 and 1000cycles	4C/703 mAhg^{-1}
[8]	Fe_2O_3/CA	Nanoparticles	0.1C/617mAhg^{-1} for 100cycles	0.8C/546 mAhg^{-1}
[9]	Fe_2O_3@C/GNs	Submicro-particles	0.2C/900mAhg^{-1} for 50cycles	
[10]	α-Fe_2O_3/VC (vulcan carbon)	Nanoparticles	0.1C/825mAhg^{-1} for 100cycles	1C/635 mAhg^{-1}
[11]	Ferrite/carbon hybrid	Nanosheets	0.1C/600mAhg^{-1} for 50cycles	
[12]	α-Fe_2O_3/C	Pseudocubic	0.2C/688mAhg^{-1} for 50cycles	
[13]	γ- Fe_2O_3@CNFs	Nanoparticles	0.05C/830mAhg^{-1} for 40cycles	5C/336 mAhg^{-1}
[14]	γ- Fe_2O_3@GNS	Nano-particle	0.1C/500mAhg-1 and 1C/200mAhg-1 for 100cycles	
[15]	Fe_2O_3@CNTS	Nanobelts	0.1C/865.9 mAhg^{-1} for 50cycles	4C/442 mAhg^{-1}
[16]	CNT-encapsulated Fe_2O_3	Nanoparticles	35 mAg^{-1}/811.4mAhg^{-1} for 100cycles	1.2C/332 mAhg^{-1}
[17]	Fe_2O_3/CNFs	Nanorod	0.2C/758mAhg^{-1} for 50cycles	10C/245 mAhg^{-1}
[18]	α-Fe_2O_3-carbon nanofibe	Nanoparticles	0.05C/604mAhg^{-1} for 100cycles	
[19]	Fe_2O_3 on graphene	Nanocrystals	0.2C/1049mAhg^{-1} for 450cycles	2C/634 mAhg^{-1}
[20]	Fe_2O_3 on graphene	Nanorods	2C/508mAhg^{-1} for 200cycles	
[21]	Fe_2O_3graphene	Sheet-on-sheet sandwich-like	1C/662.4mAhg^{-1} for 100cycles and 2C/456.2mAhg^{-1} for 100cycles	
[22]	Fe_2O_3/graphene	Nanorod-like	0.1C/602.2mAhg^{-1} for 30cycles	1C/210.7 mAhg^{-1}
[23]	Fe_2O_3/Graphene	Particles	0.05C/1092mAhg^{-1} for 50cycles	1C/501 mAhg^{-1}
[24]	Fe_2O_3/graphene	Particles	0.05C/1069mAhg^{-1} for 50cycles	1C/543 mAhg^{-1}
[25]	Graphene/ Fe_2O_3/SnO_2	Nanoparticles	0.4C/700mAhg^{-1} for 100cycles	10C/139 mAhg^{-1}

[26]	α- Fe_2O_3/RGO	Nanoparticles	0.1C/950mAhg^{-1} for 70cycles	0.8C/700 mAhg^{-1}
[27]	Iron-oxide/graphene	Nanoparticles	0.1C/900mAhg^{-1} for 50cycles	5C/500 mAhg^{-1}
[28]	40wt%RGO/γ- Fe_2O_3	Nanoparticles	0.5C/690mAhg^{-1} for 100cycles	10C/280 mAhg^{-1}
[29]	Fe_2O_3–graphene hybrid	Nanoparticles	0.05C/1000+/-50mAhg^{-1} for 100cycles	2.5C/171 mAhg^{-1}
[30]	α-Fe_2O_3/graphene	Nanoparticles	0.1C/742mAhg^{-1} for 50cycles	
[31]	RGO- Fe_2O_3	Nanospindles	0.1C/969mAhg^{-1} for 100cycles and 5C/336mAhg^{-1} for 100cycles	
[32]	Fe_2O_3/graphene	Microspheres	160 mAg^{-1} /660mAhg^{-1} for 100cycles	2.4C/332 mAhg^{-1}
Current work	Core-shell Nanohollow γ- Fe_2O_3@Graphene	Nanoparticles	1C/833mAhg^{-1} for 100cycles ; 2C/551 mAhg^{-1} for 100cycles	10C/504 mAhg^{-1}

References

1 N. Cabrera, *Philosophical Magazine*, 1949, **40**, 175.

2(a) J. C. Groen, L. A. A. Peffer and J. Pérez-Ramírez, *Microporous and Mesoporous Materials*, 2003, **60**, 1; (b) K. S. W. Sing, *Pure and Applied Chemistry*, 1985, **57**, 603.

3(a) L. A. Riley, S. Van Atta, A. S. Cavanagh, Y. Yan, S. M. George, P. Liu, A. C. Dillon and S.-H. Lee, *Journal of Power Sources*, 2011, **196**, 3317; (b) C. Wu, H. Zhang, Y. X. Wu, Q. C. Zhuang, L. L. Tian and X. X. Zhang, *Electrochimica Acta*, 2014, **134**, 18.

4 C. Wu, X. Li, W. Li, B. Li, Y. Wang, Y. Wang, M. Xu and L. Xing, *Journal of Power Sources*, 2014, **251**, 85.

5 Y. Wang, L. Yang, R. Hu, L. Ouyang and M. Zhu, *Electrochimica Acta*, 2014, **125**, 421.

6 P. Li, J. Deng, Y. Li, W. Liang, K. Wang, L. Kang, S. Zeng, S. Yin, Z. Zhao, X. Liu, Y. Yang and F. Gao, *Journal of Alloys and Compounds*, 2014, **590**, 318.

7 X. Gu, L. Chen, S. Liu, H. Xu, J. Yang and Y. Qian, *Journal of Materials Chemistry A*, 2014, **2**, 3439.

8 N. Liu, J. Shen and D. Liu, *Electrochimica Acta*, 2013, **97**, 271.

9 G. Wang, H. Wang, S. Cai, J. Bai, Z. Ren and J. Bai, *Journal of Power Sources*, 2013, **239**, 37.

10 N. K. Chaudhari, M. S. Kim, T. S. Bae and J. S. Yu, *Electrochimica Acta*, 2013, **114**, 60.

11 B. Jang, M. Park, O. B. Chae, S. Park, Y. Kim, S. M. Oh, Y. Piao and T. Hyeon, *Journal of the American Chemical Society*, 2012, **134**, 15010.

12 F. Cheng, K. Huang, S. Liu, J. Liu and R. Deng, *Electrochimica Acta*, 2011, **56**, 5593.

13 Y. Wu, P. Zhu, M. V. Reddy, B. V. Chowdari and S. Ramakrishna, *ACS Appl Mater Interfaces*, 2014, **6**, 1951.

14 O. Vargas, Á. Caballero and J. Morales, *Electrochimica Acta*, 2014, **130**, 551.

15 M. Wu, J. Chen, C. Wang, F. Wang, B. Yi, W. Su, Z. Wei and S. Liu, *Electrochimica Acta*, 2014, **132**, 533.

16 W. J. Yu, P. X. Hou, F. Li and C. Liu, *Journal of Materials Chemistry*, 2012, **22**, 13756.

17 Z. Liu and S. W. Tay, *Materials Letters*, 2012, **72**, 74.

18 L. Ji, O. Toprakci, M. Alcoutlabi, Y. Yao, Y. Li, S. Zhang, B. Guo, Z. Lin and X. Zhang, *ACS Appl Mater Interfaces*, 2012, **4**, 2672.

19 H. Zhang, L. Zhou and C. Yu, *RSC Advances*, 2014, **4**, 495.

20 T. Hu, M. Xie, J. Zhong, H. T. Sun, X. Sun, S. Scott, S. M. George, C. S. Liu and J. Lian, *Carbon*, 2014, **76**, 141.

21 J. Kan and Y. Wang, *Scientific reports*, 2013, **3**, 3502.

22 B. Zhao, R. Liu, X. Cai, Z. Jiao, M. Wu, X. Ling, B. Lu and Y. Jiang, *Journal of Applied Electrochemistry*, 2013, **44**, 53.

23 W. Xiao, Z. Wang, H. Guo, Y. Zhang, Q. Zhang and L. Gan, *Journal of Alloys and Compounds*, 2013, **560**, 208.

24 W. Xiao, Z. Wang, H. Guo, X. Li, J. Wang, S. Huang and L. Gan, *Applied Surface Science*, 2013, **266**, 148.

25 G. Xia, N. Li, D. Li, R. Liu, C. Wang, Q. Li, X. Lu, J. S. Spendelow, J. Zhang and G. Wu, *ACS Appl Mater Interfaces*, 2013, **5**, 8607.

26 M. Du, C. Xu, J. Sun and L. Gao, *Journal of Materials Chemistry A*, 2013, **1**, 7154.

27 B. Jang, O. B. Chae, S. K. Park, J. Ha, S. M. Oh, H. B. Na and Y. Piao, *Journal of Materials*

Chemistry A, 2013, **1**, 15442.

28 I. T. Kim, A. Magasinski, K. Jacob, G. Yushin and R. Tannenbaum, *Carbon*, 2013, **52**, 56.

29 L. Tian, Q. Zhuang, J. Li, C. Wu, Y. Shi and S. Sun, *Electrochimica Acta*, 2012, **65**, 153.

30 D. Chen, W. Wei, R. Wang, J. Zhu and L. Guo, *New Journal of Chemistry*, 2012, **36**, 1589.

31 S. Bai, S. Chen, X. Shen, G. Zhu and G. Wang, *RSC Advances*, 2012, **2**, 10977.

32 G. Wang, T. Liu, Y. Luo, Y. Zhao, Z. Ren, J. Bai and H. Wang, *Journal of Alloys and Compounds*, 2011, **509**, L216.